# Dislocations in charge-ordered $Pr_{0.5}Ca_{0.5}MnO_3$ epitaxial thin films prepared by a two-step growth technique

Y. L. Zhu [a]; X. Wang [a]; M. J. Zhuo [a]; Y. Q. Zhang [a];X. L. Ma [a]

[a] Shenyang National Laboratory for Materials Science, Institute of Metal Research, Chinese Academy of Sciences, Shenyang 110015, P.R. China

First published on: 23 March 2010

## PLEASE SCROLL DOWN FOR ARTICLE

Taylor & Francis
Taylor & Francis Group

# Dislocations in charge-ordered $Pr_{0.5}Ca_{0.5}MnO_3$ epitaxial thin films prepared by a two-step growth technique

Y.L. Zhu\*, X. Wang, M.J. Zhuo, Y.Q. Zhang and X.L. Ma

*Shenyang National Laboratory for Materials Science, Institute of Metal Research,
Chinese Academy of Sciences, Shenyang 110015, P.R. China*

Charge-ordered $Pr_{0.5}Ca_{0.5}MnO_3$ (PCMO) thin films epitaxially grown on $SrTiO_3$ (100) substrates were prepared by a two-step growth technique which resulted in a 10 nm thick first layer and a 70 nm thick main layer. The dislocations in the as-received films were investigated using conventional and high-resolution transmission electron microscopy. Pure-edge misfit dislocations with Burgers vectors $a\langle 011 \rangle$ and line directions $\langle 100 \rangle$ were found to be the major interfacial defects responsible for the full misfit relief in the PCMO films. These dislocations constitute a square grid of dislocation lines parallel to the PCMO/$SrTiO_3$ interface. In contrast, two types of dislocations were identified within the first layer. One is of edge type with Burgers vectors $a\langle 110 \rangle$ and line directions $\langle 001 \rangle$; the other, of screw type with Burgers vectors $a\langle 110 \rangle$ and line directions $\langle 110 \rangle$. Cross-slip of the latter may contribute to the multiplication of misfit dislocations necessary for a total misfit relaxation. Few threading dislocations were observed in the main layer. The dislocation configurations in the films are discussed in detail.

**Keywords:** dislocations; transmission electron microscopy; thin films; perovskites

## 1. Introduction

Charge ordering (CO) in the perovskite-type $Pr_{0.5}Ca_{0.5}MnO_3$ (PCMO) compound is probably one of the most captivating properties of manganites [1,2]. Such a phenomenon appears in compounds that have certain values of Ca-doping and corresponds to an ordering of the charges in two different Mn sublattices. Moreover, the insulating CO state can be totally suppressed by the application of an external magnetic field [3,4], although the magnetic field is usually quite high in the bulk materials. For example, a 25 T magnetic field is required to melt the CO state in the bulk PCMO [5]. In comparison, much lower magnetic fields (below 10 T) were employed to destroy the CO state in thin films of PCMO, which may be ascribed either to the effects of lattice strains due to the substrate [6,7] or the effects of disorder induced by strain relaxation in the PCMO films prepared by the two-step

\*Corresponding author. Email: ylzhu@imr.ac.cn

growth technique [8]. The latter is closely related to the defects in the films during their growth.

The lattice mismatch and the difference in thermal expansion coefficients between the film and the substrate result in strains, which can be employed to alter the properties of materials. This is particularly true for manganite perovskite oxides, whose electrical and magnetic properties are inherently sensitive to the defects in the material. In the earlier studies, the control of the mechanical misfit strain in PCMO films was attempted either by changing the film thickness [9], or by selecting a specific substrate [7,10]. However, the competition between strain buildup and strain relaxation (one major source for disorder) narrows the range of choice of variables (such as substrates and film thickness) to achieve the desired misfit strain in the films. In consequence, recently a two-step growth technique was introduced to accelerate strain relaxation of epitaxial perovskite-based oxide films [8,11], which proved to be an effective way of separating the influences of lattice and thermal mismatches on misfit strain. Thin films grown by such a novel technique are attractive not only for fundamental studies but also for practical applications.

On the other hand, the structure and microstructure information on these oxide materials is of great importance for understanding the interplay of structure, magnetism, and electronic transport. Transmission electron microscopy (TEM) is a powerful tool for the characterization of microstructures in materials and during the past few years, it has been widely applied to the studies of low-dimensional functional materials, and in particular, to thin films of these oxides [12–14]. Nevertheless, the microstructures and the dislocation configuration in the PCMO thin films are still not clear, especially in films prepared by the two-step growth technique.

In this article, we report on a detailed study of dislocation structures in PCMO thin films grown epitaxially on $SrTiO_3$ (STO) by the two-step growth technique. Both interfacial dislocations and dislocations within the films were observed, which constitute the major defects in these films. The formation mechanism of these defects is discussed.

## 2. Experimental

In this study, the PCMO thin films were grown on STO substrates by DC sputtering in a pure oxygen atmosphere of 300 Pa with substrate-source on-axis geometry. The sputtering rate was 1 nm/min. A ceramic target of $Pr_{0.5}Ca_{0.5}MnO_3$ with 99.999% purity was used for the thin-film deposition. The film was prepared by the two-step growth technique: a thin layer was first grown at $120°C$ up to 10 nm; then the substrate temperature was raised to $840°C$ and annealed at this temperature for 30 min. The second layer was grown under this condition up to 70 nm.

TEM specimens for both cross-sectional and plan-view observations were prepared by the conventional method, i.e. by slicing, grinding, dimpling, and finally ion-milling. Plan-view specimens were ion-milled only from the substrate side. A Tecnai G2 F30 transmission electron microscope, equipped with a high-angle annular dark-field (HAADF) detector was used at 300 kV for lattice imaging, contrast analysis, and Z-contrast imaging.

## 3. Results and discussion

### 3.1. *General information*

Bulk PCMO shows an orthorhombic symmetry with the space group *Pnma* at room temperature. The lattice parameters are $a = 0.5395$ nm $\approx a_p\sqrt{2}$, $b = 0.7612$ nm $\approx 2a_p$, and $c = 0.5403$ nm $\approx a_p\sqrt{2}$ [1], where $a_p$ is the lattice constant of the primitive cell of cubic perovskite structure, 0.38 nm. Such an orthorhombic structure is derived from the cubic phase at high temperature by tilting and/or deformation of the $MnO_6$ octahedra. On transforming, a bulk single crystal breaks up into a domain microstructure, minimizing in this way the strain energy associated with the spontaneous deformation at the unit-cell level. The number of different orientation variants depends on the ratio of the orders of the point groups of parent and product phases (which is, for instance, six in the case of $Pm3m \rightarrow Pnma$). Therefore, exactly speaking, there should be six oriented domains, although electron diffraction may only reveal three of them distinguishable [12]. In the case of thin films, the orientation of PCMO depends on the substrate. For example, the PCMO films prepared by a one-step technique on $LaAlO_3$ are [101]-oriented [10], while on $SrTiO_3$ substrate, the films are [010]-oriented [7]. Crystallographically, the [010]-oriented film indicates that the [101]* and [10$\bar{1}$]* directions of the film (in-plane parameters) are parallel to the $a^*$ and $b^*$ of STO, whereas the [010]* of the film is perpendicular to the substrate (out-of-plane parameter); while in the case of [101]-oriented, the [10$\bar{1}$]* and [020]* directions of the film (in-plane parameters) are parallel to the $a^*$ and $b^*$ of STO, whereas the [101]* of the film is perpendicular to the substrate (out-of-plane parameter). This definition is based on the plan-view observation. However, it is worth mentioning that the [101]-oriented film and the [010]-oriented one have a very similar lattice mismatch with the STO substrate, which can be calculated based on the corresponding interplanar distances. The distances $d_{101}$ and $d_{020}$ are calculated to be 0.3817 and 0.3806 nm, respectively. In this case, we assume that similar misfit relaxation process occurs in both [101]-oriented PCMO/STO and [010]-oriented PCMO/STO, just like the case of $SrRuO_3$ (SRO)/$SrTiO_3$ system [15] where orthorhombic $SrRuO_3$ is treated as pseudocubic and misfit strain relaxation is discussed by dislocation formation in $SrRuO_3/SrTiO_3$ heteroepitaxy.

For the sake of clarity, unless specified, all the diffracted vectors used in the following are referred to from the substrate of STO.

### 3.2. *Cross-sectional TEM observations*

Figure 1a shows a low-magnification HAADF image with an overview of the PCMO film on STO. HAADF mode provides incoherent images, which uses high-angle scattering and leads to strong atomic number ($Z$) contrast. The intensity of atom columns directly reflects their mean square atomic number, thus providing the composition information. The contrast in the PCMO film shown in Figure 1a is uniform, which implies that the composition variation with the film is slight. The interface between the film and substrate is distinct. The thickness of the whole film is about 80 nm, which agrees well with the expected value. Conventional TEM diffraction contrast analysis was carried out to characterize defect structures
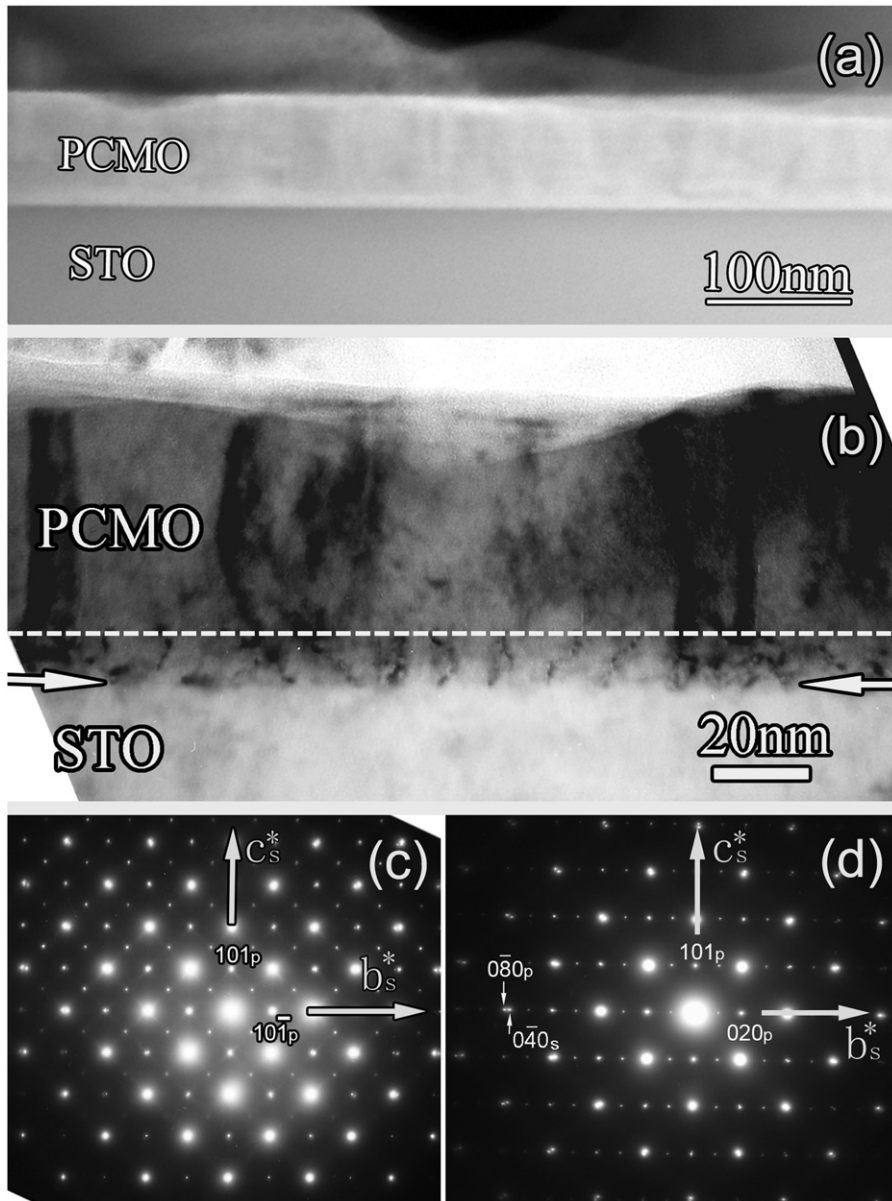
Figure 1. (a) A cross-sectional HAADF image of the PCMO film grown on the STO substrate. The uniform contrast indicates compositional homogeneity. (b) Cross-sectional bright-field image of the PCMO/STO heterostructure showing the accumulation of a high density of defects in the first layer near the interface. The separation of the first layer from the main layer of PCMO is marked by a broken line. (c) Composite EDPs of $[010]_p$ and $[100]_s$. (d) Composite EDPs of $[10\bar{1}]_p$ and $[100]_s$. Spot splitting for the PCMO and STO, due to their respective different lattice parameters, can be observed. The orthorhombic PCMO film is a mixture of both [010]-oriented and $[10\bar{1}]$ -oriented domains.
Note: Subscripts s and p denote STO and PCMO, respectively.

in the film. Figure 1b shows a cross-sectional bright-field image with the morphology of PCMO grown on STO. The interface between the film and the substrate is sharp and flat, as denoted by a pair of arrows. The location of the interface between the first layer and subsequent main layer is marked by a broken line. Besides the contrast variations in the whole film, a high density of dot-like defects is found in the area near the interface. These defects show different projected line lengths and inclination angles to the interface plane, which are associated with the TEM specimen thickness and the tilting angle. The first layer of 10 nm is crystallized, as verified by the following high-resolution transmission electron microscopy (HRTEM) observation. The fact that a large amount of defects accumulate in the first layer of PCMO implies that large misfit relaxation may be achieved during the deposition process. These defects are believed to provide nucleation sites for the film grown in the second step, leaving a large disorder in the second layer and leading to a substantial decrease of the charge-order melting field of the two-step grown film [8].

Electron diffraction experiments clarify that the as-received PCMO film is composed of both [101]-oriented and [010]-oriented domains, as shown in Figure 1c and d, taken from the areas including both the film and the substrate. The dimension of each domain is several hundreds nanometers in length, so that electron diffraction pattern (EDP) from a single domain can be obtained. Figure 1c shows a super-position of EDPs of $[010]_p$ and $[100]_s$, whereas Figure 1d shows a composite EDP of $[10\bar{1}]_p$ and $[100]_s$. The indexation of PCMO is based on an orthorhombic structure. Subscripts s and p denote STO and PCMO, respectively. Besides strong diffraction spots from the film and substrate, no extra spots can be observed, indicating that the films are free of second phase and no chemical reaction occurs along the interface. Moreover, the high-order spots splittings can be identified in Figure 1c and 1, which are due to the difference in lattice parameters of PCMO and STO. The two oriented domains share similar volume fraction in the present PCMO film, showing contrast with the results of PCMO films deposited on STO (mainly [010] domains) [7] and on $LaAlO_3$ (mainly [101] domains) [10] prepared by a normal deposition technique. It is proposed that the misfit strains between the PCMO film and its substrates influence the orientation of the orthorhombic structure [16]. When deposited on $LaAlO_3$, the misfit strain is in compression and favors the formation of the orthorhombic [101]-oriented PCMO film [7]. The PCMO film deposited on STO is [010]-oriented due to the tensile stress of the STO upon the PCMO lattice. The fact that the PCMO films in this study consist of both [101]-oriented and [010]-oriented domains may result from an inhomogeneous stress state caused by the first layer.

It is known that defect configurations play a crucial role in the performance and properties of oxide functional materials. The residual strain, which is associated with the lattice misfit relaxation in a heteroepitaxial system, has a potential influence on electrical properties. It is well known that if the lattice misfit is relatively small, films can grow coherently on substrates until a critical thickness is reached. When the film thickness exceeds the critical value, misfit dislocations form to relieve the strain. A low-magnification HRTEM image of an interface area is shown in Figure 2a, in which an array of misfit dislocation was found nearly periodically distributed along the interface. The positions of each misfit dislocation were denoted by vertical arrows. This image was obtained along [010] direction of orthorhombic PCMO or
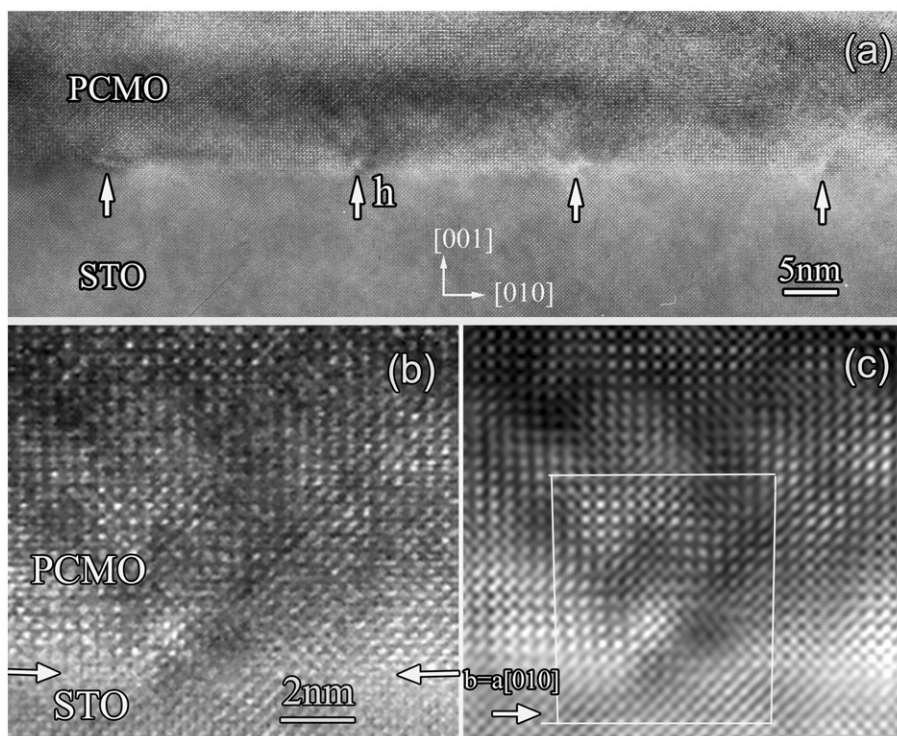
Figure 2. (a) Low-magnification cross-sectional HRTEM image of PCMO/STO hetero-epitaxy. Vertical arrows denote the positions of interfacial dislocations. (b) Enlarged pattern of the area around the dislocation ''h'' in (a). (c) Fourier-filtered image corresponding to (b), in which the Burgers circuit around the dislocation core is outlined.

[100] direction of STO. The picture clearly shows that the first layer of 10 nm has completely crystallized after annealing. Therefore it can be concluded that, even starting a growth of more or less an amorphous layer due to a low growth temperature, epitaxial conditions can be recovered in the post-annealing and the subsequent growth. One of the dislocations denoted by ''h'' in Figure 2a is selected for further character determination. Figure 2b shows the dislocation image at a larger magnification. Figure 2c shows a Fourier-filtered image corresponding to Figure 2b. By drawing a Burgers circuit around the dislocation core, the Burgers vector **b** is determined to be $a$ [010], which is the same as that in $La_{0.7}Ca_{0.3}MnO_3$ grown on STO [14].

The possible residual mismatch strain in the PCMO film with a thickness of 80 nm on STO can be estimated according to the separation distance between two adjacent misfit dislocations. Assuming that the misfit strain in this film is fully accommodated by generation of the misfit dislocations, the spacing ($S$) of misfit dislocations can be calculated based on the equation
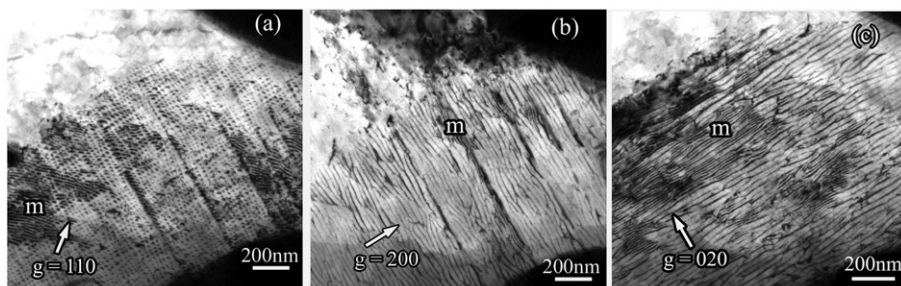
$$S = \frac{b}{f},$$

Figure 3. Plan-view TEM images of the film including the interface between the film and the substrate. All images were taken at $s > 0$ under the two-beam conditions of (a) $\mathbf{g} = (110)$, (b) $\mathbf{g} = (200)$, and (c) $\mathbf{g} = (020)$, respectively.
Note: $s$ denotes the deviation parameter and "m" the Moiré fringe. The images show strong dislocation contrast.

where $b$ is the magnitude of the Burgers vector of the misfit dislocation along the basic axis, and $f$ is the lattice misfit in the film–substrate system. The in-plane lattice constant $(d_{101})$ of PCMO thin film derived from XRD was 0.38376 nm [8], and the lattice constant of STO is 0.3905 nm. Therefore, the calculated $S$ value based on XRD is about 23 nm. In contrast, the measurement over a long distance along the interface in the TEM image indicates that the spacing is 20 nm on the average, which is very close to the value estimated based on XRD. That is to say, the as-received PCMO film is almost fully relaxed due to the formation of misfit dislocations. Such a full relaxation of strains usually does not occur in a thin film of less 100 nm prepared by conventional technique, since it is generally believed that a full relaxation of misfit strains between film and substrate is completed either by growing a large thickness of the film, or by depositing a film at quite high temperature. This study provides a clear proof that the two-step growth technique has great influence on strain relaxation.

### 3.3. *Plan-view TEM observations*

To clarify the configurations of these defects in the films, plan-view specimens were examined. Tilting experiments in conventional TEM revealed some characteristics of the misfit dislocations. Figure 3a–c shows plan-view TEM images of PCMO film, including the interface between the film and the substrate. The images were taken under $\mathbf{g} = (110)$, $\mathbf{g} = (200)$, and $\mathbf{g} = (020)$ two-beam conditions, respectively, with an incident beam direction close to [001] of the substrate. All images were recorded with the deviation parameter $s > 0$. They show strong dislocation contrast. Two arrays of dislocation lines along the [100] and [010] directions of the substrate are evident in Figure 3a with nearly equal spacings, forming a square grid of misfit dislocations. The regular distribution of misfit dislocations indicates that the strain on the growth surface is approximately uniform and no obviously preferred locations such as step or ledge, etc. exist. Figure 3b shows the image taken under $\mathbf{g} = (200)$ two-beam condition. An array of parallel dislocation lines along the [010] direction is visible. The image in Figure 3c was taken under $\mathbf{g} = (020)$. In this image, another
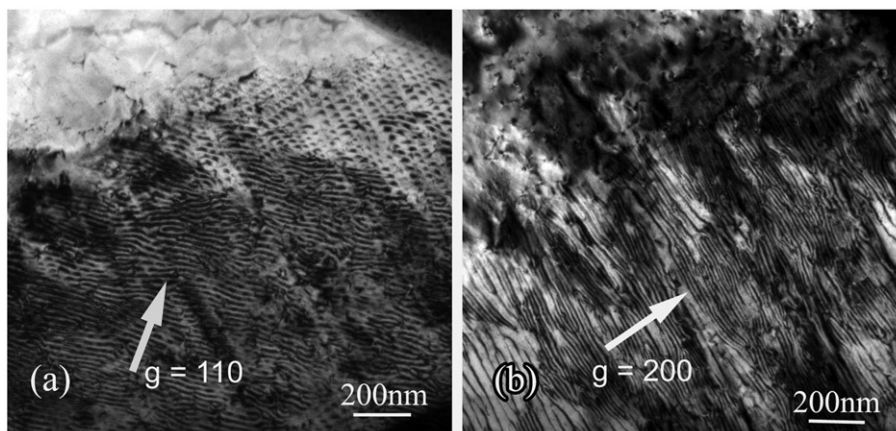
Figure 4. Plan-view bright-field images of the same region as that in Figure 3 with the operating reflections of (a) 110 and (b) 200, respectively.
Note: These two images were taken at $s \approx 0$, and show strong Moiré fringe contrast.

array of dislocation lines is visible, while those observed under $\mathbf{g} = (200)$ are invisible. According to the extinction criterion $\mathbf{g} \cdot \mathbf{b} = \mathbf{0}$, the line direction and the Burgers vector are perpendicular to each other for each misfit dislocation, indicating the presence of pure-edge dislocations. This is in agreement with the observations on other perovskite film system [15].

In addition to misfit dislocation configurations, Moiré fringes (marked with letter m in Figure 3) have been widely used to characterize the misfit systems [17–19], particularly for the study of interface between two mismatched lattices. This technique is especially appealing in that it does not require the use of high-resolution cross-sectional images to determine the Burgers vector of the misfit dislocations. Using this technique, the Burgers vector of misfit dislocations of PCMO/STO system can be determined as well. In this study, Moiré fringe are frequently observed when we tilt the specimens. The region shown in Figure 3 is again shown in Figure 4. The images were obtained at $s \approx 0$. At the Bragg condition, the intensity of the Moiré fringe contrast is so large that the dislocation contrast is nearly invisible. The fringe pattern in Figure 4a was formed by interference between the undeviated beam and a beam which had undergone one reflection of the 110 type of the substrate and one of 200 type of the PCMO film. The fringes in this pattern are perpendicular to $g_{110}$ of STO, while the fringes in Figure 4b are parallel to the visible dislocations in Figure 3b. Because the $g_{200}$ of STO are strong reflections, the spacings of the fringes in Figure 4b are half the dislocation spacing. From this, it follows that the Burgers vectors of the dislocations are equal to twice the spacing of the (200). The spacing of (200) planes of STO is $1/2$ $a[100]$, so the Burgers vectors of the misfit dislocations are $a\langle 010 \rangle$, which agrees well with the results obtained above by cross-sectional high-resolution observation. An idea of the proportion of the misfit between the two lattices that is accommodated by the misfit dislocations can be obtained by comparing the observed spacing of the Moiré fringe with the

Table 1. The observed and calculated Moiré fringe spacings from different reflecting planes.

| Reflecting planes in [010]-oriented PCMO | Reflecting planes in STO | Spacing of fringes (nm) | |
|---|---|---|---|
| | | Observed | Calculated |
| $20\overline{2}$ | 200 | $12.0 \pm 2$ | 11.4 |
| 200 | 110 | $14.5 \pm 3$ | 15.7 |

calculated ones. In the general case where the spacings of the relevant lattice plane are $d_1$ and $d_2$ and the angle between them $\phi$, the Moiré spacing $D$ is given by

$$D = \frac{d_1 d_2}{(d_1^2 + d_2^2 - 2d_1 d_2 \cos\phi)^{1/2}}.$$

This reduces to $D = d_1 d_2 / (d_1 - d_2)$, for the parallel Moiré, where $\phi = 0$.

The Moiré fringe spacings are labeled in Table 1.

It is seen that the fringe spacings obtained in experiment agree well with the calculated ones, confirming that the misfit strain between PCMO and STO is nearly fully relieved by the formation of misfit dislocations.

Figure 5 shows two plan-view bright-field images taken from other regions including both the film and the film on the thin compliant substrates (upper right). In comparison with Figures 3 and 4, in addition to the information from the interfaces, this image mainly demonstrates the feature in the PCMO thin film. The **g** vectors used for the images shown in Figure 5a and b are ($\overline{1}10$) and (110), of the STO substrate, respectively. Besides the misfit dislocations lines in the upper right corner, many small segments of dislocations can be observed, which can be better seen in the insets. Principally, they can be divided into two types: one is the dot-like dislocations denoted by A, and another is the dislocations denoted by B, which exhibit an oscillatory contrast implying that they might be inclined with respect to the film surface. Considering the defects observed in the first layer of PCMO film shown in Figure 1b, dislocations marked with A are presumably the projection of dislocations along the viewing direction with the line directions of $\langle 001 \rangle$. The subsequent HRTEM observations indicate that these dislocations have Burgers vectors $a\langle 110 \rangle$, instead of $a\langle 010 \rangle$. The latter is usually connected to the misfit dislocations of same Burgers vectors to form dislocation half-loops and be generally regarded as a major mechanism for misfit dislocation formation [20]. Since the dislocation segments lie along $\langle 001 \rangle$ direction, and have no in-plane component, type A does not contribute to the strain relaxation. The characters of those dislocations type B were also determined by the extinction criterion of $\mathbf{g} \cdot \mathbf{b} = 0$. The image in Figure 5a was taken under $\mathbf{g} = (\overline{1}10)$. Very short lines approximately along the [$\overline{1}10$] direction are visible. Figure 5b shows the image taken under $\mathbf{g} = (110)$; dislocation segments along the [110] directions are observed, while those observed under $\mathbf{g} = (\overline{1}10)$ are invisible. According to the extinction criterion $\mathbf{g} \cdot \mathbf{b} = 0$, most dislocations are those with their line directions parallel to **b**, indicating that these dislocations are screw type. By high-resolution imaging, the magnitude of the Burgers vectors of dislocations type A is also determined. Figure 6a shows
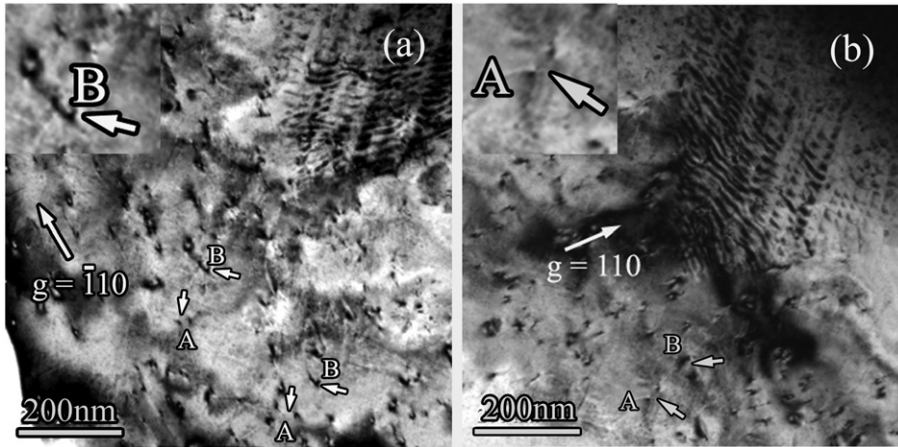
Figure 5. Plan-view TEM images taken from other regions including the film and the film on the thin compliant substrate (upper right) showing the feature in the PCMO film: (a) $\mathbf{g} = (\bar{1}10)$ and (b) $\mathbf{g} = (1\,1\,0)$.
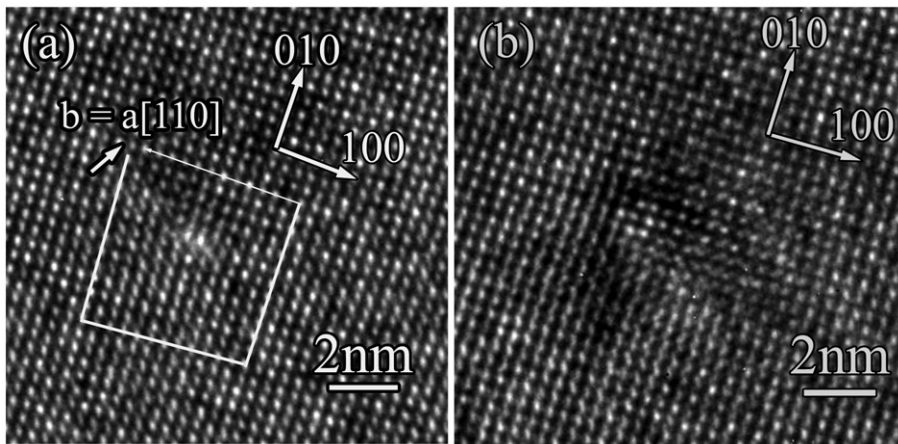Note: Two types of dislocations were identified in the PCMO thin film.



Figure 6. The [001] lattice images of (a) dislocation type A normal to the film plane with Burgers vectors $a\langle110\rangle$, and (b) dislocation type B inclined to the surface normal.

a [001] lattice image with one typical dislocation type A that lies normal to the film plane. This kind of dislocations shows relatively sharp core structure, and no dissociation can be identified. Drawing a closure surrounding the dislocation core, the Burgers vector of dislocations type A is determined as $a[110]$. The determination of Burgers vectors of dislocations type B can be considered from the energetic point of view. To have a minimum energy, these isolated dislocations should have a Burgers vector corresponding to the smallest lattice translation vectors, i.e. $a\langle100\rangle$ or $a\langle110\rangle$. Because they show a prominent contrast under $g = [110]$ in Figures 5a and b, the Burgers vectors of dislocations type B are probably $a\langle110\rangle$. Moreover, since these

Table 2. Characteristics of the major dislocations in the PCMO thin films.

| Dislocation | **l** | **b** | Character |
|---|---|---|---|
| Interfacial | $\langle 100 \rangle$ parallel to the interface | $a\langle 100 \rangle$, $\mathbf{b} \perp \mathbf{l}$ | Edge |
| Dislocation A | $\langle 001 \rangle$ perpendicular to interface | $a\langle 110 \rangle$, $\mathbf{b} \perp \mathbf{l}$ | Edge |
| Dislocation B | $\langle 110 \rangle$ inclined to surface normal | $a\langle 110 \rangle$, $\mathbf{b} \parallel \mathbf{l}$ | Screw |

Note: **b** represents the Burgers vector and **l** the direction of dislocation.

dislocations of type B inclined to the film surface (Figure 6b) and have their projected components of dislocation lines to the interface, they participate in misfit relaxation similarly to interfacial misfit dislocations.

The line directions and Burgers vectors of various dislocations observed in the PCMO films are summarized in Table 2, determined by the extinction criterion of $\mathbf{g} \cdot \mathbf{b} = 0$ and HRTEM observations.

### 3.4. *Discussion*

The equilibrium structure of an epitaxial film was calculated earlier by Van der Merwe [21]. It is known that a cross-grid array of dislocations parallel to the interfaces accommodates the lattice mismatch between film and substrate. In the recent studies on epitaxial growth of perovskite-based films, the mechanism of misfit strain relaxation and the formation of other associated defects have received much attention [22–25]. It is generally believed that a misfit dislocation is generated either from the extension of pre-existing dislocations in the substrate or from the half-loop nucleation and expansion from the film surface [15,26,27], the latter is usually the major nucleation source because of the low density of dislocations in commercial STO substrates. The first thin layer in the present PCMO film was prepared at a low temperature (120°C). It is proposed that this layer be less crystallized and should provide nucleation sites for misfit dislocation generation. The subsequent annealing leads to further crystallization of the first layer, during which the existing dislocations may move to the PCMO/STO interface and new dislocations may also form along the interface; namely, the first thin layer is served as a "template" for the subsequent growth of the epitaxial PCMO films. In this study of PCMO/STO system, most misfit dislocations were found to be edge type with Burgers vectors $a\langle 010 \rangle$ and line directions $\langle 100 \rangle$, which is also frequently observed in other epitaxial perovskite films [19,27]. In a study of misfit relaxation in $BaTiO_3$/STO heteroepitaxy system, Suzuki et al. [20] proposed a model to elaborate the generation of misfit dislocations with Burgers vectors $a\langle 010 \rangle$. In this model, threading dislocations with Burgers vectors $a\langle 110 \rangle$ are introduced from the film surface. These dislocations glide in $\{011\}$ plane down to the interface, and then are dissociated into two interfacial dislocations with Burgers vectors of $a\langle 010 \rangle$ and $a\langle 001 \rangle$, respectively. The latter does not contribute to the strain relaxation process, and may be kinetically annihilated. This process involves the diffusion of point defects. Back to this study, dislocations with Burgers vectors $a\langle 011 \rangle$ are most observed in the films (Figures 5a and b) and

show inclined contrast with the film surface. In addition, owing to the particularity of the growth technique used here, point defects initially accumulated in the first layer of PCMO may diffuse upon annealing. In the final stage, only $a\langle 010\rangle$ misfit dislocations reserve, while $a\langle 001\rangle$ interfacial dislocations disappear.

Dislocation configurations in an oxide of bulk form are usually different from those in thin films. Screw dislocations in bulk perovskite oxides have been investigated by several groups [28–30]. It was found that $a\langle 110\rangle$ screw-type dislocations in plastically deformed $SrTiO_3$ are predominant at lower temperatures [29]. A high Peierls potential or the particular core structure of screw dislocations is proposed to control the abundance of screw dislocations. In contrast, the formation of various types of dislocations in the present film is proposed to result from two-step growth, where the first layer of PCMO was deposited at low temperature (120°C).

The multiplication of the misfit dislocations is usually necessary to obtain or approach the total relaxation of heteroepitaxy systems. From the viewpoint of multiplication, not of misfit relief, cross-slip of screw dislocations is thus very important. It is discussed by Beanland [31] that single-inclined threading dislocation with one or two pinning points inside the overlayer will multiply the misfit dislocation segments through loop emission or cross-slip of screw component. As mentioned above, pure-edge threading dislocations have been frequently found in perovskite oxide thin films epitaxially grown on STO [20,27] and no screw dislocations have been reported so far except a screw component of mixed dislocations observed in lead zirconate titanate (PZT) thin films grown on SRO-coated STO by pulsed laser deposition [32]. In this study, besides edge dislocations (type A), screw dislocations (type B) are found to constitute the major dislocations in the films. The cross-slip of these dislocations is believed to facilitate the multiplication of the misfit dislocations, and thus result in the effective strain relaxation in the present system.

Few threading dislocations are observed in the main layer of PCMO thin films, as shown in Figure 1b, indicating that a reduction of threading dislocations in such a main layer is accomplished. In the previous growth of epitaxial perovskite films, a high density of threading dislocations are usually generated concomitantly with misfit dislocations [20,27], which generally degrade the physical properties of the oxide films. Romanov et al. [33] developed a model for threading dislocation reduction due to the introduction of an intentionally strained buffer layer. It is proposed that growth of thick strained layers (beyond the critical thickness) on high-quality single crystal substrate should lead to the generation of a high density of threading dislocations during strain relaxation and the motion of these threading dislocations leads to possible annihilation reactions. Indeed, a high density of dislocations was observed in the first layer of PCMO film, as shown in Figure 5. In other words, the first layer grown at low temperature is used as a buffer layer to lower the threading dislocation density in the main layer. Matthews et al. [34] also proposed that misfit strain can be used to remove threading dislocations from epitaxial thin films by driving the dislocations to the edge of the films. Multilayers are able to remove threading dislocations more effectively than single films.

The two-step growth has been widely applied to traditional semiconductor materials such as GaAs/Si. For example, the reduction of dislocation density in

GaAs/Si was achieved either by introducing a strained-layer superlattice of $In_xGa_{1-x}As$–$GaAs_yP_{1-y}$ [35] or by employing AlAs/GaAs double amorphous buffer [36]. Actually, the so-called two-step growth was initially developed for improving the crystal quality of GaAs epilayers on Si substrate. We applied this technique to grow PCMO films not only for the improvement of films but also for effective strain relaxation of the lattice misfit between PCMO and STO, which plays a critical role in altering physical properties of functional thin film materials.

## 4. Summary

The dislocations in the PCMO thin films deposited on (100) STO by two-step growth technique were characterized by TEM and HRTEM. An orthogonal array of pure edge misfit dislocations with Burgers vectors $a\langle010\rangle$ is the major characteristic at the interface between the film and the substrate. Such a formation of misfit dislocations results in a nearly full strain relaxation of PCMO/STO heterostructure. The major defects accumulated in the first 10 nm thick layer are dislocations with two types: one is of edge type with Burgers vectors $a\langle110\rangle$ and line directions of $\langle001\rangle$; the other, of screw type with Burgers vectors $a\langle110\rangle$ and line directions of $\langle110\rangle$. The screw dislocations may cross-slip to enhance the multiplication of misfit dislocations for a total strain relaxation. Few threading dislocations are observed in the 70 nm thick layer grown at the second step, thanks to the introduction of the first strained layer.

## Acknowledgements

## References

[1] Z. Jirak, S. Krupicka, Z. Simsa, M. Dlouha and S. Vratislav, J. Magn. Magn. Mater. 53 (1985) p.153.
[2] B. Raveau, M. Hervieu, A. Maignan and C. Martin, J. Mater. Chem. 11 (2001) p.29.
[3] Y. Tomioka, A. Asamitsu, H. Kuwahara and Y. Moritomo, Phys. Rev. B 53 (1996) p.R1689.
[4] Y. Tomioka, A. Asamitsu, Y. Moritomo, H. Kuwahara and Y. Tokura, Phys. Rev. Lett. 74 (1995) p.5108.
[5] M. Tokunaga, N. Miura, Y. Tomioka and Y. Tokura, Phys. Rev. B 57 (1998) p.5259.
[6] W. Prellier, Ch. Simon, B. Mercey, M. Hervieu, A.M. Haghiri-Gosnet, D. Saurel, Ph. Lecoeur and B. Raveau, J. Appl. Phys. 89 (2001) p.6612.
[7] W. Prellier, A.M. Haghiri-Gosnet, B. Mercey, Ph. Lecoeur, M. Hervieu, Ch. Simon and B. Raveau, Appl. Phys. Lett. 77 (2000) p.1023.
[8] Y.Q. Zhang, Y.L. Zhu, Z.D. Zhang and J. Aarts, J. Appl. Phys. 101 (2007) p.063919.
[9] Z.Q. Yang, Y.Q Zhang, J. Aarts, M.-Y. Wu and H.W. Zandbergen, Appl. Phys. Lett. 88 (2006) p.072507.
[10] A.M. Haghiri-Gosnet, M. Hervieu, Ch. Simon, B. Mercey and B. Raveau, J. Appl. Phys. 88 (2000) p.3545.

[11] T. Yamada, K.F. Astafiev, V.O. Sherman, A.K. Tagantsev, D. Su, P. Muralt and N. Setter, J. Appl. Phys. 98 (2005) p.054105.
[12] X.L. Ma, Y.L. Zhu, X.M. Meng, H.B. Lu, F. Chen, H. Chen, G.Z. Yang and Z. Zhang, Philos. Mag. A 82 (2002) p.1331.
[13] O.I. Lebedev, G. Van Tendeloo, S. Amelinckx, F. Razavi and H.-U. Habermeier, Phil. Mag. A 81 (2001) p.797.
[14] J.Q. He, C.L. Jia, J. Schubert and R.H. Wang, J. Cryst. Growth 265 (2004) p.241.
[15] S.H. Oh and C.G. Park, J. Appl. Phys. 95 (2004) p.4691.
[16] W. Prellier, E.R. Buzin, B. Mercey, Ch. Simon, M. Hervieu and B. Raveau, J. Phys. Chem. Solids 64 (2003) p.1665.
[17] H. Wang, S.R. Foltyn, P.N. Arendt, Q.X. Jia and X. Zhang, Physica C 444 (2006) p.1.
[18] J.E. Angelo, J.N. Kuznia, A.M. Wowchak, P.I. Cohen and W.W. Gerberich, Appl. Phys. Lett. 59 (1991) p.63.
[19] S. Auzary, F. Pailloux, M.F. Denanot and R.J. Gaboriaud, Thin Solid Films 319 (1998) p.163.
[20] T. Suzuki, Y. Nishi and M. Fujimoto, Phil. Mag. A 79 (1999) p.2461.
[21] J.H. Van der Merwe, J. Appl. Phys. 41 (1970) p.4725.
[22] J.S. Speck and W. Pompe, J. Appl. Phys. 76 (1994) p.466.
[23] J.S. Speck, A. Seifert, W. Pompe and R. Ramesh, J. Appl. Phys. 76 (1994) p.477.
[24] J.S. Speck, A.C. Daykin, A. Seifert, A.E. Romanov and W. Pompe, J. Appl. Phys. 78 (1995) p.477.
[25] P.A. Langjahr, F.F. Lange, T. Eagner and M. Rühle, Acta Mater. 46 (1998) p.773.
[26] H.P. Sun, W. Tian, X.Q. Pan, J.H. Haeni and D.G. Schlom, Appl. Phys. Lett. 84 (2004) p.3298.
[27] Y.L. Qin, C.L. Jia, K. Urban, J.H. Hao and X.X. Xi, J. Mater. Res. 17 (2002) p.3117.
[28] W. Sigle, C. Sarbu, D. Brunner and M. Rühle, Phil. Mag. 86 (2006) p.4809.
[29] Z.L. Zhang, W. Sigle and W. Kurtz, Phys. Rev. B 69 (2004) p.144103.
[30] X. Guo, Z.L. Zhang, W. Sigle, E. Wachsman and R. Waser, Appl. Phys. Lett. 87 (2005) p.162105.
[31] R. Beanland, J. Appl. Phys. 72 (1992) p.4031.
[32] I. Vrejoiu, G . Le Rhun, N.D. Zakharov, D. Hesse, L. Pintilie and M. Alexe, Phil. Mag. 86 (2006) p.4477.
[33] A.E. Romanov, W. Pompe, S. Mathis, G.E. Beltz and J.S. Speck, J. Appl. Phys. 85 (1999) p.182.
[34] J.W. Matthews, A.E. Blakeslee and S. Mader, Thin Solid Films 33 (1976) p.253.
[35] T. Nishimura, K. Mizuguchi, N. Hayafuji and T. Murotani, Jpn. J. Appl. Phys. 26 (1987) p.L1141.
[36] W.Y. Uen and T. Nishinaga, J. Cryst. Growth 128 (1993) p.52.